Spin-wave instability threshold in single-crystal yttrium iron garnet for oblique pumping

Y. H. Liu[a] and C. E. Patton
Department of Physics, Colorado State University, Fort Collins, Colorado 80523

(Received 10 September 1981; accepted for publication 8 December 1981)

The spin-wave instability threshold h_{crit} for oblique pumping in high-quality single-crystal yttrium iron garnet (YIG) at room temperature and 9.317 GHz, has been examined. The experimental dependence of h_{crit} on the pump angle indicates that the microwave field components parallel and perpendicular to the dc field operate independently in exciting spin-wave instability. Theoretical fits to the data, based on this result, indicate that the spin-wave linewidth is strongly wave vector dependent and that the wave vector dependence varies with the pump angle.

PACS numbers: 75.30.Ds, 75.50.Gg, 76.50. + g

I. INTRODUCTION

Since Suhl[1] and Schlömann[2] developed the spin-wave instability theory of nonlinear effects in ferromagnetic insulators, many theoretical and experimental results on spin-wave instability phenomena have been reported. Several papers in recent years by Jantz and coworkers[3–6] have reported interesting new nonlinear effects for parallel pumping and subsidiary absorption in single crystal yttrium iron garnet (YIG). These include fine structure,[3,4] spin-wave switching,[5] and wave-vector clamping.[6] From the work on parallel pumping in Ref. 5, and perpendicular pumping (subsidiary absorption) in Ref. 6, it appeared that the empirical wave-vector k dependence of the spin-wave linewidth ΔH_k required to fit the experimental data varied with the microwave pumping configuration. In other words, $\Delta H_k(\mathbf{k})$ changed as one changed the microwave field h_{rf} from parallel to perpendicular, relative to the static field H_{dc}. In the present study, measurements of the spin-wave instability threshold microwave field amplitude h_{crit} versus the dc field were taken for first-order processes for a range of angles between h_{rf} and H_{dc} from 0° to 90°. The data reveal a systematic variation in $\Delta H_k(\mathbf{k})$ with pump angle. More importantly, however, the study indicates that the parallel and perpendicular pumping processes operate independently rather than cooperatively. These results are elaborated upon in the sections to follow.

II. EXPERIMENT AND RESULTS

The experimental setup was similar to that of Ref. 6. The data were obtained on a single-crystal YIG sphere at room temperature, and a frequency of 9.317 GHz, with a modified Varian 4500 microwave spectrometer. A block diagram of the microwave system is shown in Fig. 1. The reference arm allows the detection diode to be biased at a few hundred mV independent of the microwave power level incident on the cavity containing the sample. The phase shifter is adjusted to obtain a proper phase relationship between the power reflected from the cavity as h_{rf} exceeds the threshold value and the reference signal. The cavity iris is adjusted for critical coupling of the cavity below threshold. One improvement over Ref. 6 is that the cavity Q was accurately measured[7] and the incident power was calibrated with a microwave power meter in place of the cavity. From these calibration parameters, the absolute values of h_{rf} as a function of the precision attenuator setting could be determined by the usual microwave cavity perturbation theory. In Ref. 6 all data were in terms of relative h_{rf} values.

The data were obtained in a manner similar to that described in Ref. 6. The sample used for all of the results reported here was a high-quality YIG single crystal 0.707-mm-diam sphere with a fine polished surface and a ferromagnetic resonance (FMR) x-band linewidth of about 0.4 Oe. The sample was free to rotate in the sample holder tube and care was taken to ensure that the static field was always along the easy [111] direction. The cavity-sample configuration was such that the linear polarized microwave field was in the $(1\bar{1}0)$ plane at an angle $0° < \Psi < 90°$ to the static field. The raw data consisted of recorded sheets each with a family of curves of detector voltage versus the dc field amplitude as shown in Fig. 2. Successively higher curves are for higher power levels, indicated in db down relative to the highest power of 0.490 W. Since, in the absence of instability, the power reflected from the critically coupled cavity is zero,

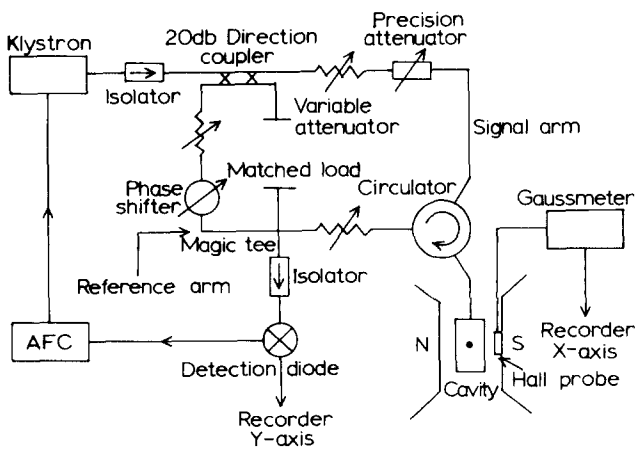

FIG. 1. Block diagram of the microwave spectrometer used to measure the instability thresholds.

[a]Visiting research associate on leave from the Physics Department, Shangdong University, People's Republic of China.

 0021-8979/82/075116-06$02.40 © 1982 American Institute of Physics

Downloaded 09 May 2003 to 129.82.31.230. Redistribution subject to AIP license or copyright, see http://ojps.aip.org/japo/japcr.jsp

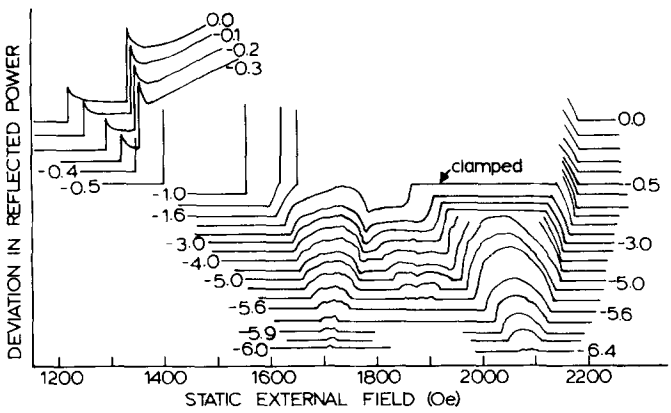

FIG. 2. Typical recorder traces demonstrating the acquisition of instability data.

portions of the curves for h_{rf} below threshold are simply horizontal lines. As the dc field is changed to values such that h_{rf} (held constant) is above threshold, the curves break. Each break point, therefore, yields a value of h_{crit} and the dc field at which that instability occurs.

From a careful measurement of the break points as a function of H_{dc}, a curve of h_{crit} versus static field may be constructed. Such a curve is shown for parallel pumping by the solid points in Fig. 3. The gradual decrease in h_{crit} with increasing field and the sharp cusp at about 1520 Oe are typical of so-called butterfly curves for parallel pumping on narrow linewidth single crystals. Above the cusp, h_{crit} increases, but the curve is decorated by some extra dips. These dips at about 1630, 1700, and 1800 Oe appear to be due to magnetoelastic interactions as will be discussed in the next section.

In Figs. 4–7, the solid points indicate butterfly curves for pump angles of 20°, 40°, 60°, and 90°, respectively. The solid lines represent theoretical fits to be discussed in the next section. In following the evolution of the experimental butterfly curves as the pump angle is varied from 0° to 90°, several observations are in order. First, the parallel pumping minimum retains its static field position and cusp-like character at all angles for which h_{rf} has a parallel component, e.g., all angles except 90°. As this component decreases, the

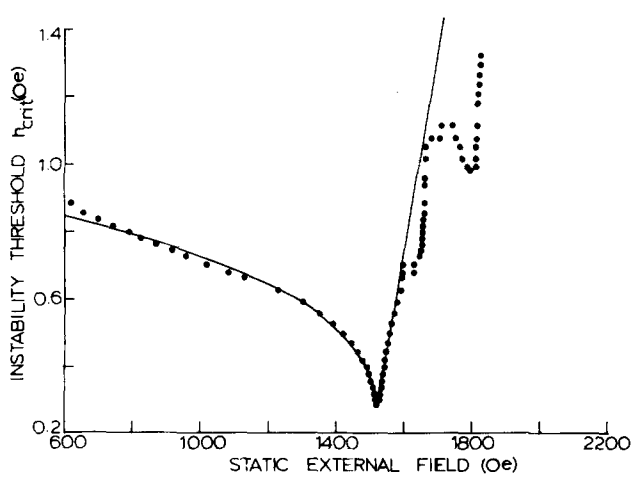

FIG. 3. Experimental (solid points) and theoretical butterfly curve for parallel pumping.

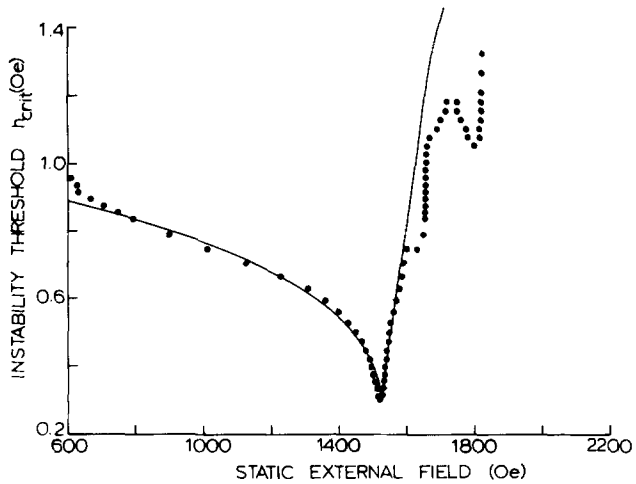

FIG. 4. Experimental (solid points) and theoretical butterfly curve for oblique pumping at $\Psi = 20°$.

value of h_{crit} at the minimum increases.

Second, the same comments apply to the perpendicular pumping minimum at about 2120 Oe. It retains its static field position and rounded character, shows up for all angles for which h_{rf} has a perpendicular component, and the value of h_{crit} at the minimum increases as the perpendicular component of h_{rf} becomes smaller. These behaviors have several profound implications concerning instability theory, as will be discussed in the next section.

Third, a close examination of the data shows that at one particular value of the static field, 1650 Oe, the value of h_{crit} is 0.94 Oe, independent of the pump angle. One may say that this point serves as a kind of center of gravity for the entire family of butterfly curves. For lower static fields, h_{crit} is generally increasing with pump angle. For higher static fields, h_{crit} is generally decreasing with pump angle.

A final empirical observation has more to do with the detailed character of the instability onset, as indicated by the break points in Fig. 2. It was noted in Ref. 6 that the breaks were sharp but continuous for moderate power levels, but changed to sharp, abrupt jumps for larger h_{crit} values (Fig. 2 of Ref. 6). Similar effects were found in the present study, as shown in Fig. 8 for perpendicular pumping. It is seen that as

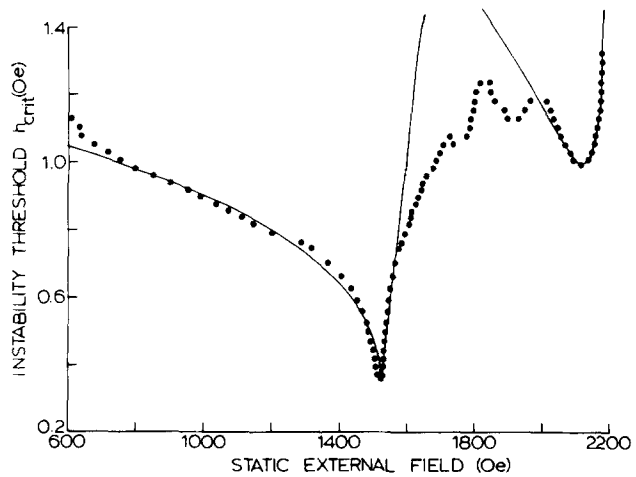

FIG. 5. Experimental (solid points) and theoretical butterfly curve for oblique pumping at $\Psi = 40°$.

Downloaded 09 May 2003 to 129.82.31.230. Redistribution subject to AIP license or copyright, see http://ojps.aip.org/japo/japcr.jsp

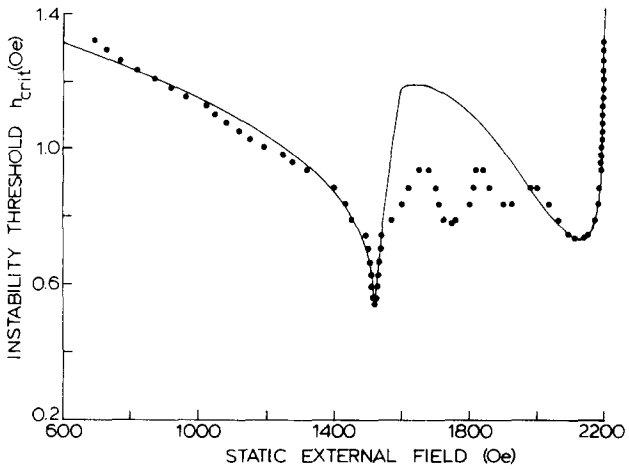

FIG. 6. Experimental (solid points) and theoretical butterfly curve for oblique pumping at $\Psi = 60°$.

the power is increased above about 1.1 db (h_{crit} of 1.167 Oe), the instability onset character changes to an abrupt jump. At higher power levels, two jumps are actually observed. The second onset appears to represent a second spin-wave mode instability.

III. DISCUSSION AND THEORETICAL ANALYSIS

The butterfly curve data presented in the previous section has been analyzed using a generalized instability theory for linear oblique pumping[8] which includes the influence of crystalline anisotropy and the **k** dependence of the spin-wave linewidth on the threshold. In the limiting cases of parallel pumping ($\Psi = 0°$) and perpendicular pumping ($\Psi = 90°$), the published theory appears to be adequate. In the case of intermediate angles, however, it appears that the parallel and perpendicular components of h_{rf} act independently in producing instability. The two processes do not appear to be coupled as expected from theoretical considerations.[8,9,10] With a suitable modification, theoretical analysis of the data for all angles yields a systematic evolution of the **k** dependence of the spin-wave linewidth ΔH_k versus Ψ. These three cases, parallel pumping, perpendicular pumping, and oblique pumping are considered below.

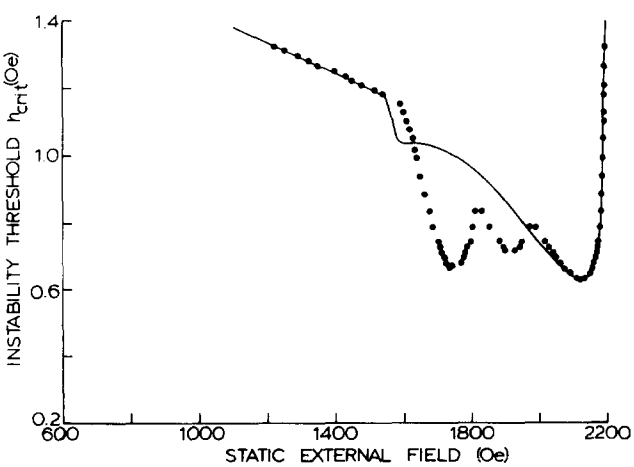

FIG. 7. Experimental (solid points) and theoretical butterfly curve for perpendicular pumping.

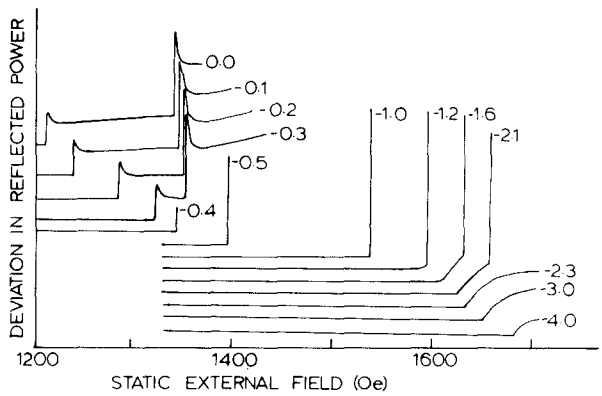

FIG. 8. Typical recorder as in Fig. 2 traces but on an expanded field scale to show the change in character of the instability onset.

A. Parallel pumping

The theoretical spin-wave instability threshold microwave field amplitude h_{crit} for parallel pumping is given by[2]

$$h^{\parallel}_{crit} = \min\left(\frac{\omega}{\omega_m}\frac{\Delta H_k}{\sin^2\theta_k}\right), \tag{1}$$

where ω is the pump frequency in rad/s, ω_m is $\gamma 4\pi M_s$ with γ the gyromagnetic ratio (1.76×10^7 Oe^{-1} s^{-1}) and $4\pi M_s$ the saturation induction (1 780 G), and θ_k is the angle between the spin-wave wavevector **k** and the static field direction. The minimization is with respect to all allowed spin-waves for a given value of static field at a frequency $\omega_k = \omega/2$. The θ_k for such spin-waves is specified by the dispersion relation

$$\omega_k = \gamma[(H_i + Dk^2)(H_i + Dk^2 + 4\pi M_s \sin^2\theta_k)]^{1/2}, \tag{2}$$

where H_i is the static internal field including demagnetization and anisotropy fields. The crystalline anisotropy also modifies the form but not the substance of Eqs. (1) and (2). In the interest of clarity, these effects have been neglected in the discussion to follow. For the actual calculations, the rigorous formulas were incorporated, following Ref. 8 for $\Psi = 0°$. Below the cusp position in Fig. 3, the minimum $h^{\parallel}_{crit}$ is for $\theta_k = 90°$, with k determined by Eq. (2); k increases from $k = 0$ at the cusp as H_{dc} is reduced.

Following Ref. 6, a phenomenological function for the spin-wave linewidth,

$$\Delta H_k = A_0 + A_1 \sin^2 2\theta_k + B_1 L(k/B_2), \tag{3}$$

with

$$L(x) = \frac{1}{1.39x}\ln\left(1 + \frac{8x^2(1+2x^2)}{1+8x^2}\right), \tag{4}$$

was incorporated in Eq. (1) to obtain theoretical curves for comparison with the data in Fig. 3. This functional form has no rigorous theoretical justification but, as noted in Ref. 6, the θ_k and k dependences are loosely consistent with the three-magnon relaxation calculation of Sparks.[11]

The parameters A_0, A_1, B_1, and B_2 were varied to achieve an optimum fit to the data of Fig. 3 with

$A_0 = 0.151$ Oe, $A_1 = 0.383$ Oe,

$B_1 = 0.505$ Oe, and $B_2 = 3.5\times 10^6$ cm^{-1},

Downloaded 09 May 2003 to 129.82.31.230. Redistribution subject to AIP license or copyright, see http://ojps.aip.org/japo/japcr.jsp

the solid curve in Fig. 3 was obtained. Below the cusp position, the fit is good except for low fields for which the sphere is not magnetized to saturation. The good fit extends for about 100 Oe above the cusp until the extra dips are encountered.

Additional measurements indicate that these extra dips are magnetoelastic in origin. The approach was to squeeze slightly on the sphere to put it under a small compressive stress and repeat the measurements. The resulting butterfly curve is shown in Fig. 9. It is seen that compression causes the high field dips to weaken substantially and also causes a new dip to show up about 70 Oe below the main cusp. This new dip is precisely at the field position for crossover of the $\omega_k = \omega/2$, $\theta_k = 90°$ magnons dispersion curve and the transversal phonons dispersion branch. A related "phonon notch" has been extensively studied in the past[12,13] and it is interesting that a "phonon dip" can be induced in single crystal YIG at x band and room temperature by a moderate compressive stress. The precise origin of the extra dips above the cusp is not known. They could possibly be due to standing wave acoustic modes at the spin-wave frequency, just as the extra dips under perpendicular pumping in Fig. 7 and in Ref. 6 are due to standing-wave magnetostatic modes at $\omega/2$.

B. Perpendicular pumping

Much of the preceeding discussion also is applicable to perpendicular pumping, except that the pertinent equation is given by

$$h^{\perp}_{\text{crit}} = \min\left(\frac{\omega}{\omega_m}\frac{\Delta H_k}{\sin\theta_k \cdot \cos\theta_k}\frac{1}{F(\theta_k)\alpha(H,\omega)}\right), \quad (5)$$

where $\alpha(H,\omega)$ designates the normalized uniform precesson or ferromagnetic resonance amplitude and $F(\theta_k)$ is given by

$$F(\theta_k) = \tfrac{1}{2}[(\omega_m{}^2 \sin^4\theta_k + \omega^2)^{1/2} - \omega_m \sin^2\theta_k] + \omega/2\,. \quad (6)$$

Strictly speaking, the linearly polarized microwave pump field introduces a dependence of h_{crit} on the azimuthal spin-wave angle ϕ_k. In the interest of clarity, this complication is ignored in the discussion. The rigorous analysis of Ref. 8 has been used in generating the theoretical curves, however.

The selection of a suitable trial $\Delta H_k(\mathbf{k})$ function which would give a reasonable fit to the data presented a problem. The form in Eq. (3) which was found to work quite well for perpendicular pumping in Ref. 6 did not turn out to work very well here. The problem appears to be in the different shapes of the experimental curves around the minimum relative to the values of h_{crit} at the kink point. The sample used in Ref. 6 was somewhat larger. In any event, it was found that two separate functions were needed, one for $k = 0$ and one for $k \neq 0$.

$$\Delta H_k = A_0 + A_1 \sin^2 2\theta_k,\ k = 0\,, \quad (7)$$

$$\Delta H_k = A_2 + B_1 L(k/B_2),\ k \neq 0\,. \quad (8)$$

The coefficients in Eqs. (7) and (8) were adjusted to yield an optimum fit to the data of Fig. 7. The values which yielded the solid curve in the figure are

$$A_0 = 0.151 \text{ Oe}, A_1 = 0.383 \text{ Oe}, A_2 = 0.310 \text{ Oe}\,,$$

$$B_1 = 0.282 \text{ Oe, and } B_2 = 1.7\times10^5 \text{ cm}^{-1}\,.$$

The fit in the linear region below 1520 Oe and around the minimum above 2000 Oe is quite good. The two dips in the experimental curve at 1740 and 1915 Oe are caused mainly by magnetostatic mode interactions as discussed in Ref. 6. The theoretical kink at 1540 Oe is about 50 Oe lower than shown by the data. The sphere squeezing experiment under perpendicular pumping indicates that this discrepancy is also related to the magnetoelastic interaction. Figure 10 shows the perpendicular pumping butterfly curve for the sphere subjected to a small compressive stress. The squeezing causes the experimental kink to move down in static field by precisely the amount needed to match the theory!

C. Oblique pumping

Oblique pumping at angles between 0° and 90° for h_{rf} relative to H_{dc} has been considered by several authors.[8,9,14,15,16] The essential result was that the parallel and perpendicular components act cooperatively in producing the instability, with h_{crit} given theoretically by an equation of the form

$$\frac{1}{h^{\text{obl}}_{\text{crit}}} = \max\left(\frac{\cos\Psi}{h^{\parallel}_c} + \frac{\sin\Psi}{h^{\perp}_c}\right), \quad (9)$$

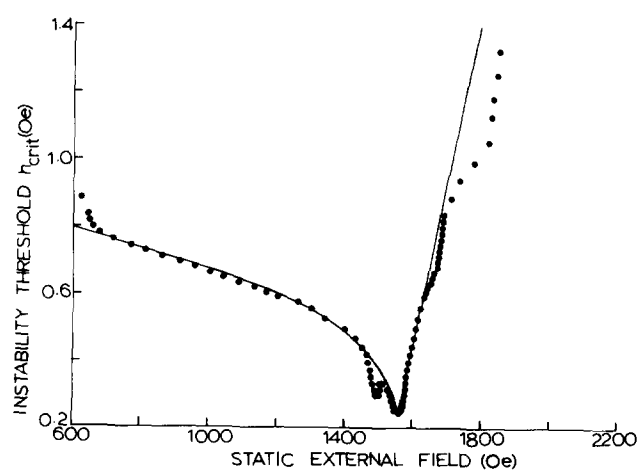

FIG. 9. The same as Fig. 3 except that the data points were obtained with the sphere under a small compressive stress.

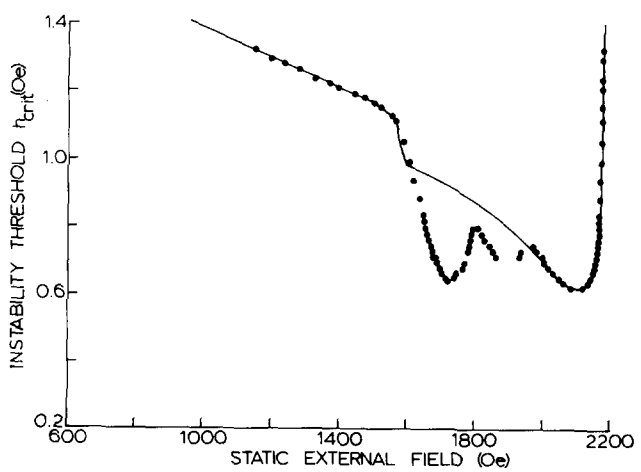

FIG. 10. The same as Fig. 7 except that the data points were obtained with the sphere under a small compressive stress.

Downloaded 09 May 2003 to 129.82.31.230. Redistribution subject to AIP license or copyright, see http://ojps.aip.org/japo/japcr.jsp

where $h_c^{\parallel}$ and $h_c^{\perp}$ are given by the expressions in the large parentheses in Eqs. (1) and (5), respectively.

It appears, however, that cooperative pumping does not occur for narrow linewidth single crystal YIG but that the parallel and perpendicular components of h_{rf} act independently. This conclusion is obtained by examining the variation of $h_{\rm crit}$ at the parallel pump cusp position (1520 Oe) and $h_{\rm crit}$ at the perpendicular pump minimum position (2120 Oe) versus pump angle. For an independent parallel pump process, $h_{\rm crit}^{(1520)}$ versus Ψ should lie on a curve generated by plotting $h_{\rm crit}^{\parallel\text{-cusp}}/\cos\Psi$ versus Ψ, where $h_{\rm crit}^{(1520)}$ is the threshold field at 1520 Oe for any pump direction Ψ, and $h_{\rm crit}^{\parallel\text{-cusp}}$ is just the threshold field at 1520 Oe in Fig. 3. For an independent perpendicular pump process, $h_{\rm crit}^{(2120)}$ versus Ψ should lie on the curve generated by plotting $h_{\rm crit}^{\perp\text{-min}}/\sin\Psi$ versus Ψ, where $h_{\rm crit}^{(2120)}$ is the threshold field at 2120 Oe for any pump direction Ψ, and $h_{\rm crit}^{\perp\text{-min}}$ is just the threshold field at 2120 Oe in Fig. 7 (or Fig. 10).

Figure 11 shows that $h_{\rm crit}$ follows precisely the scenario given above. Except for a small fall off at 75° and 80° for $h_{\rm crit}^{(1520)}$, the experimental threshold points fall right on the theoretical curves. If the pumping processes were acting cooperatively, the data points would all lie somewhat below the solid curves, as discussed in Ref. 9 and apparent from Eq. (8) above. The reason for this behavior is not known. The theory for oblique pumping of Refs. 8 and 9 follows the original approach of Suhl and Schlömann and shows that the processes *should be* cooperative.

As a further test of the independent pumping conclusion, attempts were made to fit theoretical curves to the experimental data for the intermediate angles. Fits based on Eq. (9) were very poor for many reasonable trial functions for $\Delta H_k(k)$.

As an alternative, the $h_{\rm crit}^{\rm obl}$ expression was modified to take independent pumping into account for the entire butterfly curve. This expression,

$$h_{\rm crit}^{\rm obl} = \min\left(\frac{h_{\rm crit}^{\parallel}}{\cos\Psi}, \frac{h_{\rm crit}^{\perp}}{\sin\Psi}\right), \tag{10}$$

was found to give quite satisfactory fits to the data for all of the intermediate pump angles, except for the field interval

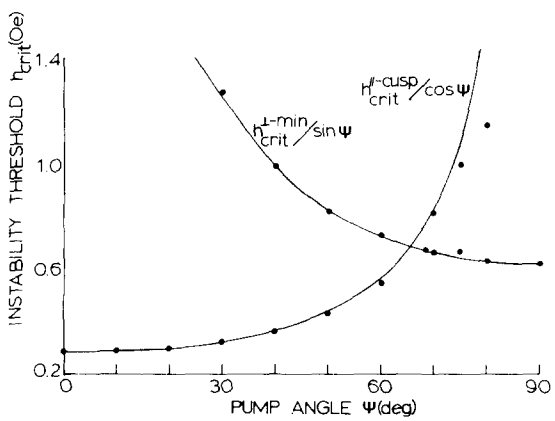

FIG. 11. Plots of threshold field amplitudes vs pump angle as discussed in text to demonstrate the role independent pumping process in oblique pumping for single crystal YIG.

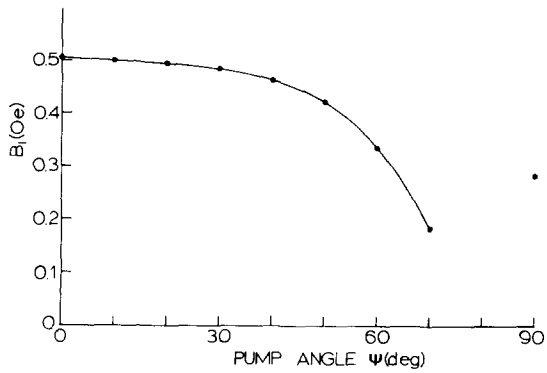

FIG. 12. Variation of the spin-wave linewidth B_1 parameter with pump angle as discussed in text.

1600–2000 Oe where magnetoelastic and magnetostatic mode interactions complicate matters.

The fits shown in Figs. 4, 5, and 6 for $\Psi = 20°$, 40°, and 60°, respectively, by the solid curves (and for other angles as well) were based on the same trial function for ΔH_k as used for parallel pumping. It was necessary, however, to allow the B_1 parameter to vary with angle as indicated in Fig. 12. The values of A_0, A_1, and B_2 were the same as for parallel. It is remarkable that the fits are so good, especially for the high field portions of the curves where the perpendicular pump process is dominant. For each pump angle shown, one particular $\Delta H_k(\mathbf{k})$ function suffices to fit both the parallel pump dominant and the perpendicular pump dominant regions. Of course, the reason for a change in $\Delta H_k(\mathbf{k})$ with pump angle is still theoretically unresolved.

IV. SUMMARY AND CONCLUSION

Spin-wave instability effects in high-quality single crystal YIG have been examined experimentally and theoretically as a function of the pump angle between the linearly polarized microwave field and the static dc field. The data and the analysis show that the parallel and perpendicular components of the microwave field work independently to promote the parallel pumping instability and the perpendicular pumping instability, respectively. Thus, at any given dc field and pump angle the observed threshold is for the process with the lowest threshold. In general (except for 0° and 90°), parallel pumping dominates at low fields and perpendicular pumping dominates at high fields. At intermediate fields, the experimental results show that extra dips occur due to magnetoelastic interactions, as well as local minima due to magnetostatic modes.

Several important unresolved problems have been revealed by the present study. Most important, the theoretical reason for independent parallel and perpendicular pumping processes needs clarification. The present result is purely empirical. The existing theory consistently indicates that the pumping should be cooperative. A second problem concerns the **k**-dependence of the spin-wave linewidth. While it is satisfying that one function can account for both the parallel and perpendicular instability portions of a butterfly curve at a given pump angle, it is not at all clear why that function should change with pump angle.

Finally, the role of compressive stress in suppressing or

Downloaded 09 May 2003 to 129.82.31.230. Redistribution subject to AIP license or copyright, see http://ojps.aip.org/japo/japcr.jsp

enhancing magnetoelastic interactions with respect to spin-wave instability needs considerable clarification. The extra dips which appear above the parallel pump cusp for no stress, but weaken under stress, need to be identified. The phonon-crossover dip which appears just below the cusp for the sample under stress needs further study. In other works, this crossover shows up as an increase in h_{crit}, the so-called "Turner notch." Why is it enhanced, but changed to a dip under stress at x-band and room temperature? Why does compressive stress cause the experimental kink point to move to lower field? These questions should be researched further.

ACKNOWLEDGMENTS

The authors are grateful to Dr. W. Tolksdorf and H. Clausen, Philips Research Laboratories, Hamburg, for providing the several YIG samples used in this study, to Dr. W. Jantz for helpful comments on the results, and to Professor L. M. Silber for a careful reading and comments on the manuscript. Y. H. Liu was supported on an exchange program of the People's Republic of China. The work was supported in part by the Army Research Office, Contract No. DAAG29-80K-0084.

[1]H. Suhl, J. Phys. Chem. Solids **1**, 209 (1957).
[2]E. Schlömann, J. J. Green, and V. Milano, J. Appl. Phys. **31**, 3865 (1960).
[3]W. Jantz, dissertation, Universität Freiburg, 1974.
[4]W. Jantz and J. Schneider, Phys. Status Solidi A **31**, 595 (1975).
[5]C. E. Patton and W. Jantz, IEEE Trans. Magn. **MAG-14**, 698 (1978).
[6]C. E. Patton and W. Jantz, J. Appl. Phys. **50**, 7082 (1979).
[7]Z. Frait and C. E. Patton, Rev. Sci. Instrum. **51**, 1092 (1980).
[8]C. E. Patton, Phys. Status Solidi B **92**, 211 (1979).
[9]J. J. Green, C. E. Patton, and E. Stern, J. Appl. Phys. **40**, 172 (1969).
[10]C. E. Patton, J. Appl. Phys. **40**, 2837 (1969).
[11]M. Sparks, *Ferromagnetic Relaxation Theory* (McGraw-Hill, New York 1964), p. 91.
[12]See *Physics of Magnetic Garnets*, edited by A. Paoletti (North Holland, Amsterdam, 1978), p. 490.
[13]E. H. Turner, Phys. Rev. Lett. **5**, 100 (1960).
[14]C. E. Patton, J. Appl. Phys. **41**, 431 (1970).
[15]L. V. Kitaev, A. A. Goncharova, and G. I. Katamaran, Fiz. Tverd. Tela (Leningrad) **9**, 330 (1967). [Sov. Phys. Solid State **9**, 246 (1967).]
[16]Y. M. Yakovlev, Fiz. Tverd. Tela (Leningrad) **10**, 2431 (1968). [Sov. Phys. Solid State **10**, 1911 (1969).]

Downloaded 09 May 2003 to 129.82.31.230. Redistribution subject to AIP license or copyright, see http://ojps.aip.org/japo/japcr.jsp